photonics

MDPI

Review

Review of a Specialty Fiber for Distributed Acoustic Sensing Technology

Yixiang Sun, Hao Li, Cunzheng Fan, Baoqiang Yan, Junfeng Chen, Zhijun Yan and Qizhen Sun *

National Engineering Laboratory for Next Generation Internet Access System (NGIA), Wuhan National Laboratory for Optoelectronics (WNLO), School of Optical and Electronic Information, Huazhong University of Science and Technology, Wuhan 430074, China; m202072360@hust.edu.cn (Y.S.); lhbeyond@hust.edu.cn (H.L.); buckt@hust.edu.cn (C.F.); yanbaoqiang@hust.edu.cn (B.Y.); junfengchen@hust.edu.cn (J.C.); yanzhijun@hust.edu.cn (Z.Y.)

* Correspondence: qzsun@mail.hust.edu.cn

Abstract: Specialty fibers have introduced new levels of flexibility and variability in distributed fiber sensing applications. In particular, distributed acoustic sensing (DAS) systems utilized] the unique functions of specialty fibers to achieve performance enhancements in various distributed sensing applications. This paper provides an overview of recent preparations and developments of specialty-fiber-based DAS systems and their sensing applications. The specialty-fiber-based DAS systems are categorized and reviewed based on the differences in scattering enhancement and methods of preparation. The prospects of using specialty fibers for DAS systems are also discussed.

Keywords: specialty fibers; distributed acoustic sensing; DAS; distributed fiber sensor; scattering enhancement fiber

Citation: Sun, Y.; Li, H.; Fan, C.; Yan, B.; Chen, J.; Yan, Z.; Sun, Q. Review of a Specialty Fiber for Distributed Acoustic Sensing Technology. *Photonics* **2022**, *9*, 277. https://doi.org/10.3390/photonics9050277

Received: 29 January 2022
Accepted: 15 March 2022
Published: 20 April 2022

1. Introduction

The identification of the internal properties of a medium is an important way to understand nature and explore the world, which can be obtained using both direct and indirect measurements. Regarding acoustic waves, the transmission form of sound travels in different directions with the help of various media in the environment. Therefore, the internal properties of the medium can be recognized by measuring and tracking the information carried by the acoustic field [1–3]. In recent years, acoustic sensing technology has been widely used in the analysis of material properties at different scales, such as in geological structure detection [4], resource exploration [5], structural health monitoring [6], and perimeter security [7].

Acoustic sensors allow people to analyze media through acoustic information. With the increases in the range and scale of acoustic detection, the demand for distributed high-capacity acoustic sensors is also expanding. Furthermore, distributed acoustic sensing (DAS) has become a research hotspot because of its advantages in terms of anti-electromagnetic interference, high sensitivity [8], and the small volume and light weight of the systems. DAS is a rising acoustic sensing technology that uses passive optical fibers as the transmission and sensing medium at the same time, squeezing information from optical fiber Rayleigh backscatters to achieve acoustic detection in the surrounding environment. Most DAS systems are based on phase-sensitive optical time domain reflectometry (φ-OTDR), since the phase change in Rayleigh backscattered light has a linear relationship with the acoustic wave acting on the optical fiber [9].

Common DAS systems usually use a single-mode fiber (SMF) as the sensing fiber. However, with such fibers the Rayleigh backscattered light is extremely weak and the signal-to-noise ratio (SNR) of the optical sensing signal is low, which leads to a poor SNR of the demodulation phase signal in DAS systems based on φ-OTDR [10]. In addition, since a laser pulse with a narrow linewidth and high coherence is injected into the fiber, the

interference between the Rayleigh scattering points in one pulse will produce interference cancellation, resulting in coherent fading of the backscattered light, forming a "dead zone" on the sensing fiber [11]. In recent years, in order to solve the defects of the poor SNR values and the sensitivity of phase demodulation in SMF-DAS systems, many suppression technologies for noise have been studied, such as coherent fading, while at the same time the complexity and cost of the systems has increased, leading to sacrifices in terms of the response frequency band and sensing distance [12–18]. Furthermore, it is also important to enhance the performance of the sensing fiber itself. The development of a specialty fiber for DAS technology will have broad prospects.

This paper intends to provide a comprehensive review of the different sensing features and performance enhancements provided by the specialty fibers that are used in DAS systems. The principle of the DAS technology is introduced in Section 2, followed by a discussion of the specialty-fiber-based DAS system with enhanced sensing capability and performance in Section 3. Firstly, two types of specialty fibers are introduced, a continuous scattering-enhanced (CSE) fiber and discrete scattering-enhanced (DSE) fiber, with the latter one being more widely used because of its ability to completely suppress coherent fading. Secondly, several fabrication techniques for introducing scattering enhancement points (SEP) into the fiber are summarized, including femtosecond writing and UWFBG inscription. Thirdly, a variety of methods to enhance the performance of DAS systems for discrete scattering are reviewed. Fourthly, the applications of the specialty fiber DAS system are reviewed in Section 4. Lastly, the prospects of using specialty fibers for DAS systems are discussed in Section 5.

2. Fundamental Principle

2.1. Principle of DAS Technology

DAS is achieved by measuring the optical phase change caused by the axial strain variation of the optical fiber [19]. When the sound wave acts on the fiber, the fiber will produce axial strain, which changes the phase of the Rayleigh backscattering signal in the fiber. According to the photoelastic effect, there is a linear relationship between the axial strain and the optical phase change:

$$\Delta\varphi = \beta\left[1 - \frac{n^2}{2}(P_{12} + 2P_{11})\right]\Delta L \tag{1}$$

where β is the propagation constant of light, n is the refractive index of the optical fiber, P_{12} and P_{11} are tensor coefficients of the optical fiber, ΔL is the change in fiber length from equation $\Delta L = \varepsilon_s L$, ε_s is the axial strain of the fiber, and L is the length of the fiber. Thus, as shown in Figure 1, as long as the changes in the phase difference between the two points A and B of the probe light can be extracted, the changes in axial strain can be known and the quantitative perception of acoustic waves or vibrations can finally be measured. It is crucial for DAS to achieve distortion-free phase demodulation in all positions of the fiber.

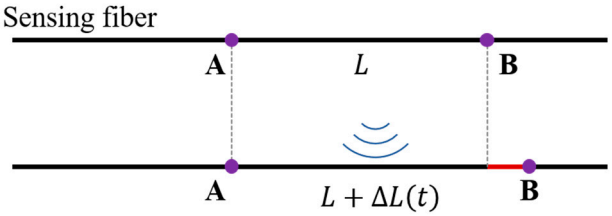

Figure 1. The sensing principle of the fiberoptic DAS.

Since Rayleigh scattering is an elastic scattering method without any nonlinear effect, and as the Rayleigh scattered light at different positions can be distinguished via the time of reflection back to the fiber launch end, the optical fiber phase extraction technique based on phase-sensitive optical time domain reflection (φ-OTDR) is widely used in DAS systems [20,21]. In 2011, using heterodyne coherent detection technology, the phase of the

Rayleigh scattering signal was successfully demodulated for the first time [22]. The scheme of the heterodyne coherent detection is shown in Figure 2. The local oscillator light and the Rayleigh scattering signal at point A can be expressed as:

$$E_{LO} = A_{LO}exp[j2\pi ft + j\varphi_{LO}] \tag{2}$$

$$E_A = A_A exp[j2\pi(f + \Delta f)t + j\varphi_A] \tag{3}$$

where A_{LO} and A_A are the amplitude of the local oscillator light and the Rayleigh scattering signal at point A, f is the frequency of the probe light, Δf is the frequency shift of the pulse modulator, φ_{LO} and φ_A are the optical phases of the local oscillator light and the Rayleigh scattering signal at point A, respectively. After these two signals are coupled by a 3 dB coupler and interfere with the photosensitive surface of the balanced photoelectric detector (BPD), the light intensity detected by the BPD can be expressed as:

$$I \propto 2E_{LO}E_A cos(\Delta ft + \varphi'_A) \tag{4}$$

where $\varphi'_A = \varphi_A - \varphi_{LO}$ is the phase difference between the two signals. Then, φ'_A can be calculated using a digital coherent IQ demodulation algorithm. Similarly, φ'_B can also be calculated at point B by the same algorithm. Through the spatial differential calculation of the phase, the phase difference φ_{AB} between two points A and B can be finally obtained, which linearly shows the axial strain of the optical fiber and finally allows the quantitative perception of sound waves and vibrations.

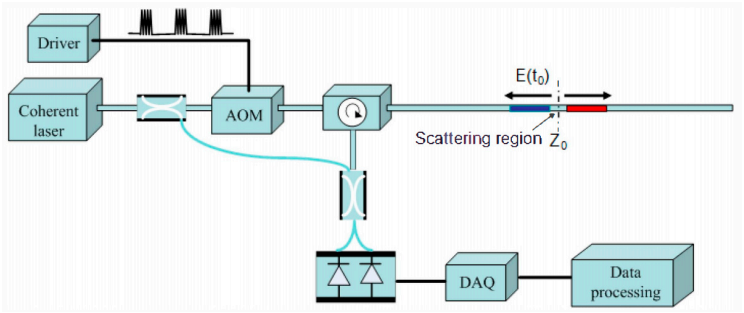

Figure 2. Typical heterodyne coherent detection scheme [22].

In addition to the heterodyne-based coherent detection scheme, researchers have also proposed other phase demodulation schemes, such as the 3 × 3 coupler scheme [23], phase-generated carrier (PGC) [24], and linear frequency sweeping pulse method [25]. Some representative schemes are shown in Figure 3, all of which can achieve distributed optical phase demodulation.

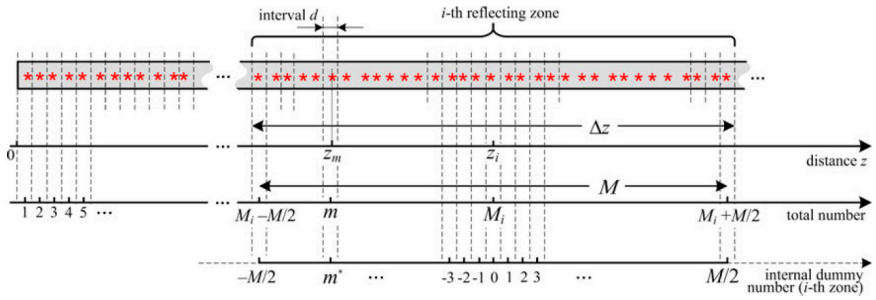

Figure 3. Rayleigh scattering model of the single-mode optical fiber [26].

2.2. Limitations of Single-Mode Fiber (SMF) DAS

Despite SMF DAS technology having been applied in many fields, such as geological monitoring, pipeline monitoring, and oil exploration, and with the advantages of

distributed detection, high spatial resolution, and high sensitivity, it still has been limited by interference fading and poor signal consistency. The reasons are analyzed below.

In particular, when the pulse width is narrow enough, the Rayleigh backscattering signals of point A and B as discussed in Section 2.1 can be obtained according to the arrival time of the Rayleigh backscattering light. In fact, the probe pulse has a certain pulse width, and the Rayleigh scattering signals of different scattering points in the pulse width will interfere with each other because of the high coherence of the probe light. The interference result of the Rayleigh scattering can only represent a section fiber near point A and B. Due to the inhomogeneous doping in the preparation of the optical fiber, the interference phenomenon of the Rayleigh scattering is random, which will inevitably affect the phase demodulation performance. In order to describe the Rayleigh scattering phenomenon in SMF accurately, researchers established a SMF scattering model [26].

The Rayleigh scattering model is shown in Figure 4. First, the SMF is discretized and the nonuniform distribution of impurities in the core is regarded as a series of equivalent Rayleigh scattering points (ERSP) of micron or submicron size, which are numbered as 1, 2, 3, $\cdots$, M, respectively. Each backscattering coefficient and the position of the scattering point can be presented as (a_m, z_m); that is, the M-th scattering point is on z_m, while the reflectivity is a_m. Since the ERSP can be regarded as the superposition of multiple scattering points with a smaller scale, its position can be expressed as $z_m = md + \Delta d$, where Δd obeys the uniform distribution in $\left[-\frac{d}{2}, \frac{d}{2}\right]$ and a_m obeys the Rayleigh distribution. According to the above analysis, the Rayleigh scattering signal received at the i-th time can be expressed as the superposition of interference of the Rayleigh scattering signal of a section of fiber:

$$E_i = \sum_{z_{i1} < z_m < z_{i2}} A a_m \cdot \exp\left(j \frac{2\pi}{\lambda} \cdot 2n z_m\right) \tag{5}$$

where n is the refractive index of the fiber, z_{i1} and z_{i2} are related to the pulse width, which satisfies $z_{i2} - z_{i1} = Wc/2n$, W is the pulse width of the probe pulse, and c is the speed of light in vacuum. Researchers have also verified this model [8]; when the interference signal involves interference cancellation, the signal intensity $|E_i|$ will become weaker, leading to a worse optical SNR. Further, the light intensity declines to the same level as the acquisition noise and the demodulated phase information will be submerged in the noise, forming a blind detection area, which is called interference fading. In addition, due to the randomness of the reflectivity a_m of the equivalent scattering point, the equivalent positions of the signals received at different times are different. The signal received at time i in Equation (5) is taken as an example. Since the scattered signal at this time is the superposition of multiple complex numbers, its intensity Aa_m is the mode of the complex number, and the phase $j\frac{2\pi}{\lambda} \cdot 2nz_m$ related to position z_m is the argument for the complex number, so Equation (5) can be expressed as the superposition of multiple vectors. As depicted in Figure 4, when the Rayleigh scattering intensity of the front-end equivalent scattering point is strong, the signal received at time i can be regarded as Rayleigh scattering near the z_{i1} position, while when the Rayleigh scattering intensity of the back-end equivalent scattering point is strong, the signal received at the same time can be regarded as Rayleigh scattering near the z_{i2} position.

In general, it is the randomness of the intensity and position of Rayleigh scattering of ordinary single-mode fibers that leads to the problems of interference fading and poor signal time consistency in DAS, making it difficult to perform high-fidelity sound wave tracking when analyzing the internal properties of the medium.

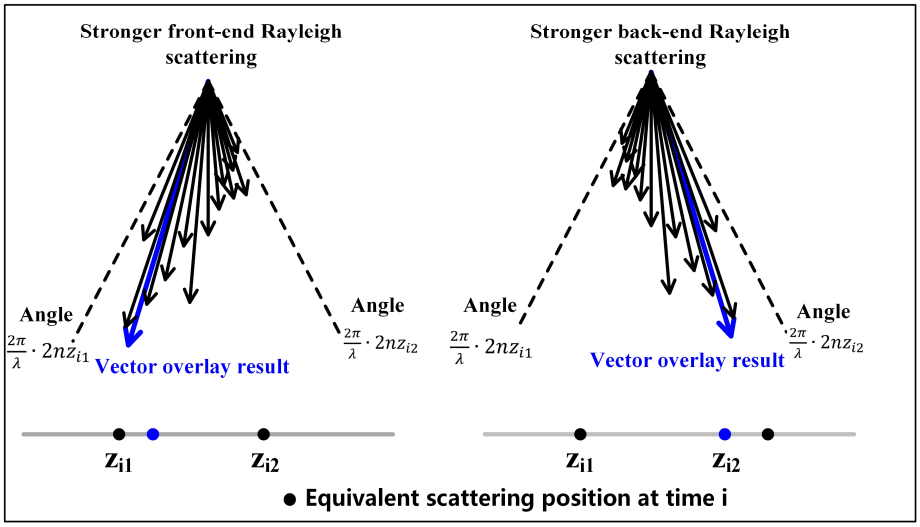

Figure 4. Schematic diagram of equivalent scattering positions in pulse interference.

3. Reviews of Specialty-Fiber-Based DAS Technology

In order to solve the interference fading and poor consistency in SMF DAS, researchers have conducted a series of studies [13,27–30]. Among them, the most effective method is to improve the fibers to enhance the fiber backscattering, such as continuous scattering-enhanced fibers and discrete scattering-enhanced fibers formed by inscribing microstructures into the fibers. In addition, due to the characteristics of microstructure optical fibers, researchers also designed and improved the matching optical scheme to improve the performance of the DAS system. In this section, a comprehensive review of the specialty-fiber-based DAS with enhanced sensing capability and performance is presented.

3.1. Continuous Scattering-Enhanced Fiber-Based DAS

Continuous scattering enhancement (CSE) allows the suppression of coherent fading by enhancing the Rayleigh scattering of the whole fiber, whose essence is to enhance the scattering intensity a_m of the ERSP model described in Section 2.2 by doping or writing continuous grating in the fiber, so as to enhance the light intensity after interference superposition, finally allowing the suppression of interference fading.

In 2017, the OFS laboratory in the United States used the phase mask method to efficiently and continuously inscribe Bragg gratings in multicore fibers through ultraviolet (UV) exposure. The backscattering intensity of the fiber was increased by 14 dB, and the reflection spectrum is shown in Figure 5a. Then, in cooperation with Fotech in the UK, CSE fiber was used in a DAS system, and the SNR of 1 km of CSE fiber was increased by 15 dB [31–34]. Although this method effectively improves the SNR, the bandwidth of the Bragg grating reflection spectrum is narrow, and the reflection wavelength will drift with temperature and stress variation. When the external environment changes, the wavelength of the incident light and grating reflection may not correspond to each other, resulting in the loss of the scattering enhancement effect. Therefore, the application range of this kind of fiber is limited and cannot be used in fields where high temperature and high pressure are required on site. In addition to inscribing continuous gratings, changing the fiber doping is another way to increase the intensity of the Rayleigh scattering. In 2018, Butov et al. used nitrogen-doped fiber as the sensing fiber, which increased the SNR of the acoustic wave detection by 3 dB [35]. In the same year, Feng S et al. used an erbium-doped optical fiber for distributed optical fiber sensing, adopted a phase-generated carrier (PGC) optical scheme, which converts homodyne interference into heterodyne interference by modulating the frequency of the signal, decreased the phase noise by 14 dB, and achieved a high-SNR acoustic measurement on 1.9 km optical fiber [36].

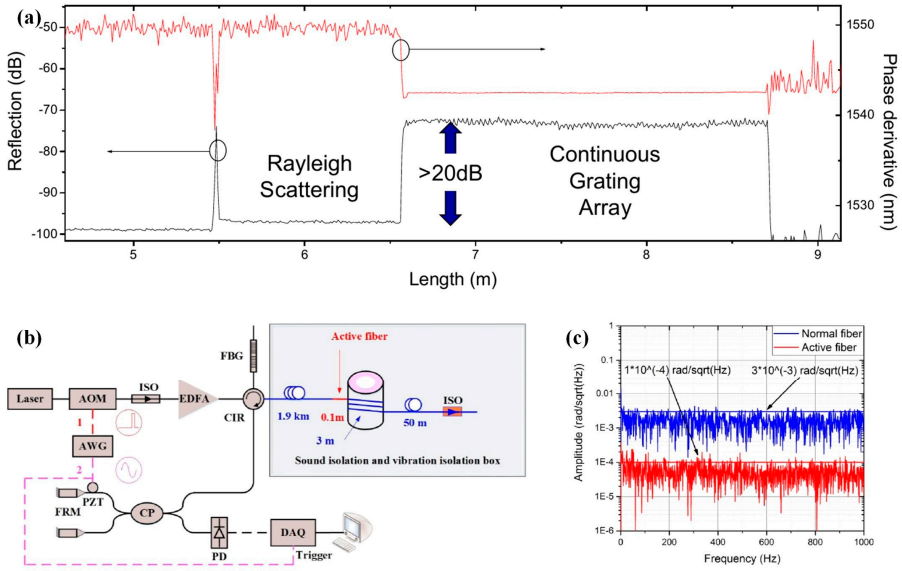

Figure 5. Typical scheme of continuous scattering-enhanced optical fiber [33,36]: (**a**) the backscattering signal distribution of a typical continuous scattering-enhanced fiber; (**b**) scheme of improved Rayleigh scattering achieved by changing the fiber doping; (**c**) scattering spectrum of high Rayleigh scattering fiber.

For the CSE scheme, although it can effectively improve the scattering intensity and suppress the coherent fading noise, the enhanced fiber scattering results in doubling of the light loss, which greatly limits the detection distance. Taking the optical fiber doping scheme as an example, if the front-end SNR is increased by 10 dB, the Rayleigh scattering of the fiber needs to be increased by ten times, which reduces the detectable distance to 1/10. More importantly, the SCE fiber does not fundamentally change the nature of the optical interference in the pulse, and still cannot completely eliminate the coherent fading phenomenon.

3.2. Discrete Scattering-Enhanced Fiber Based DAS

In addition to continuous scattering enhancement, more researchers are focusing on the application of discrete scattering-enhanced (DSE) fiber in DAS. As shown in Figure 6, the essence of this fiber is to enhance the scattering intensity of one single ERSP with a certain interval in the model illustrated in Section 2.2. The intensity of the scattering-enhanced points (SEP) is far greater than that of the ordinary ERSP. In this way, the Rayleigh scattering interference light containing the SEP can be expressed as:

$$E_i = \sum_{z_{i1}<z_m<z_{i2}, z_m \neq z_j} a_m \cdot \exp\left(j\frac{2\pi}{\lambda}\cdot 2nz_m\right) + a_j \cdot \exp\left(j\frac{2\pi}{\lambda}\cdot 2nz_j\right) \quad (6)$$

where the j-th ERSP is the scattering enhancement point. Because the scattering intensity of the SEP is much larger than that of the ordinary ERSP, the first term of the above formula can be ignored, which shows that the Rayleigh scattering signal is only determined by the SEP. Through the phase demodulation method in Section 2.1, the phase difference between the two SEP can be accurately obtained, and because of its high scattering intensity and high SNR, the interference fading can be completely eliminated, ensuring the good consistency of the signal.

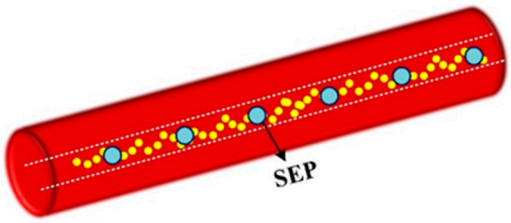

Figure 6. Schematic diagram of discrete scattering-enhanced fiber.

To verify its effectiveness, we have theoretically analyzed the DSE model and the SMF scattering model. According to the parameters shown in Table 1, three SEPs are set at 3, 7, and 11 m on the fiber at intervals of 4 m. Figure 7a,b shows the distribution results of the scattering intensity obtained from the simulation. It can be seen that the DES fiber completely suppresses the random variation of the signal amplitude and interference fading. To further explore the suppression effect of the DSE fiber on the phase noise, we solve the phase differences between 3 and 7 m on the SMF and DSE fibers, respectively, the of which results are shown in Figure 7c. Compared with SMF, the DSE fiber is not affected by the random distribution of ordinary ERSPs, but is determined by the position of the SEPs, so the phase noise is greatly suppressed.

Table 1. Parameters of discrete enhanced scattering model.

Fiber Length	Spacing of SEP	Pulse Width	Spacing of ERSP d	Repeat Times
13 m	4 m	20 ns	1 um	100

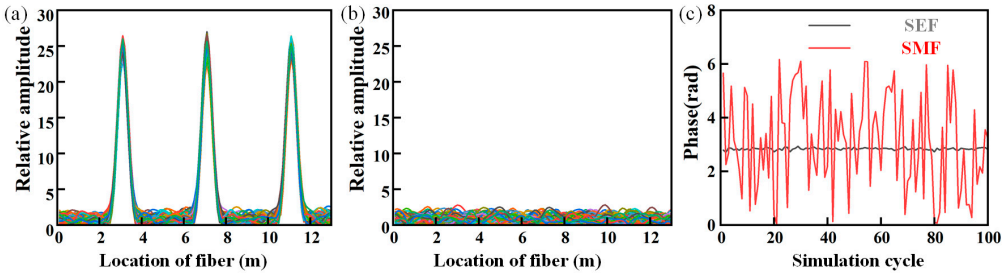

Figure 7. Simulation results of discrete enhanced scattering model: (**a**) reflection distribution of discrete enhanced fiber; (**b**) reflection distribution of single mode fiber; (**c**) phase demodulation result.

3.3. Preparation and Implementation of DSE Fiber

At present, there are two ways to manufacture the discrete scattering-enhanced fiber, one is by inscribing the periodic ultra-weak Bragg grating (UWFBG) array [29,37] into the fiber, and the other is by introducing a local wavelength-independent weak reflection array into the fiber [38–40].

UWFBG usually involves the use of ultraviolet light [41–43] or a femtosecond laser [44,45] to form a permanent periodic change in the refractive index of the optical fiber, so as to allow the backward reflection of a specific light wavelength. The most classic preparation system is shown in Figure 8a [46]. In the process of fiber drawing, through strict dynamic control, the UWFBG was written using the phase mask method, using periodic interference fringes of the ±1st diffraction light to irradiate the photosensitive fiber and periodically change the refractive index of the fiber core. Additionally, an FBG writing platform was mounted on the draw tower near the first coating to weaken vibrations in the fiber. The preparation results are shown in Figure 8b [47], and the scattering rate of the scattering-enhanced array is much higher than that of the single-mode fiber. However, as a Bragg grating method, UWFBG is sensitive to temperature and stress. When the temperature and strain of the environment are changed, the reflection wavelength of the UWFBG will drift. As shown in Figure 8c, the bandwidth of UWFBG is usually less than

2 nm and the central wavelength is determined according to the light source used in the specific experiment. Due to the limited bandwidth of UWFBG, there may be a mismatch between the reflective spectrum of UWFBG and the wavelength of the detection light when the UWFBG array fiber operates in special environments, such as for large temperature vibrations or high pressure, while the fiber will also suffer from twisting or pulling forces, meaning the reflection power from the UWFBG will degenerate into Rayleigh scattering, resulting in a blind sensing area. This characteristic of UWFBG hinders its application in underground, underwater, and other special environments [48,49].

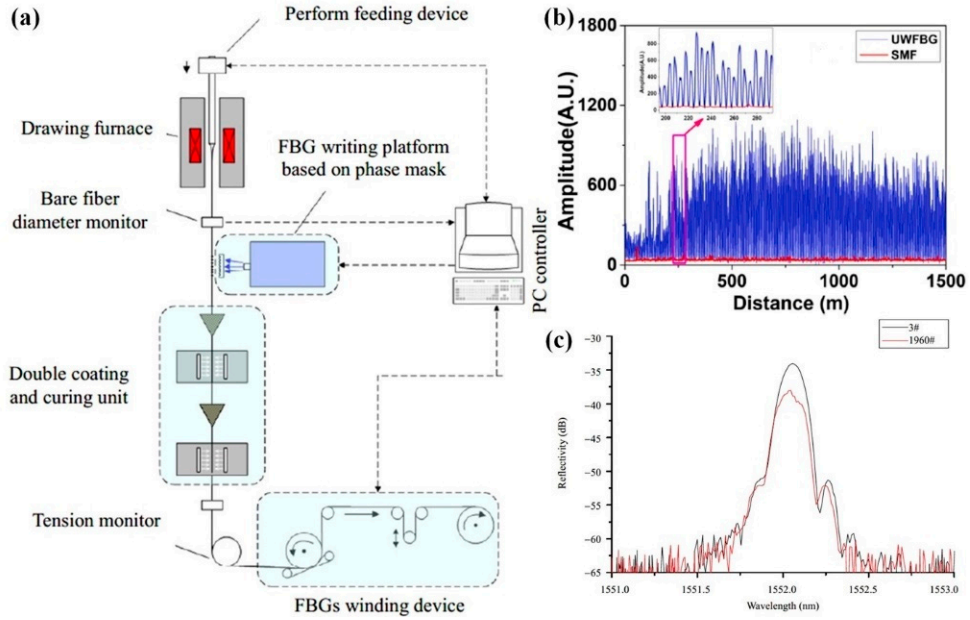

Figure 8. Typical UWFBG preparation method: (**a**) online UWFBG preparation system [46]; (**b**) OTDR measurement results of the UWFBG array [47]; (**c**) reflection spectrum of UWFBG [46].

In recent years, the enhancement scheme of a local achromatic weak reflection array has also been used in DAS [50,51]. In order to prepare a more universal discrete scattering enhancement array, Sun et al. proposed a preparation method for microstructured optical fibers with a colorless reflection point. The mechanism of the microstructure involves the local refractive index change through UV exposure without the help of the phase mask to form a Fresnel reflecting surface. The fabrication system is shown in Figure 9a [52], while the preparation results are shown in Figure 9b–d [53]. A discrete scattering enhancement array with an interval of 5 m and 15 dB enhanced intensity was achieved. When the temperature changes, the scattering intensity of the microstructure is extremely stable. In addition, the University of Southampton and other universities in the UK also used a femtosecond laser to prepare a weak reflection array [40]. The preparation system, scheme, and results are shown in Figure 10. Compared with UWFBG, whose reflection bandwidth is limited, the weak reflection points are directly engraved in the optical fiber, without wavelength selectivity, avoiding the influence of temperature and strain [54].

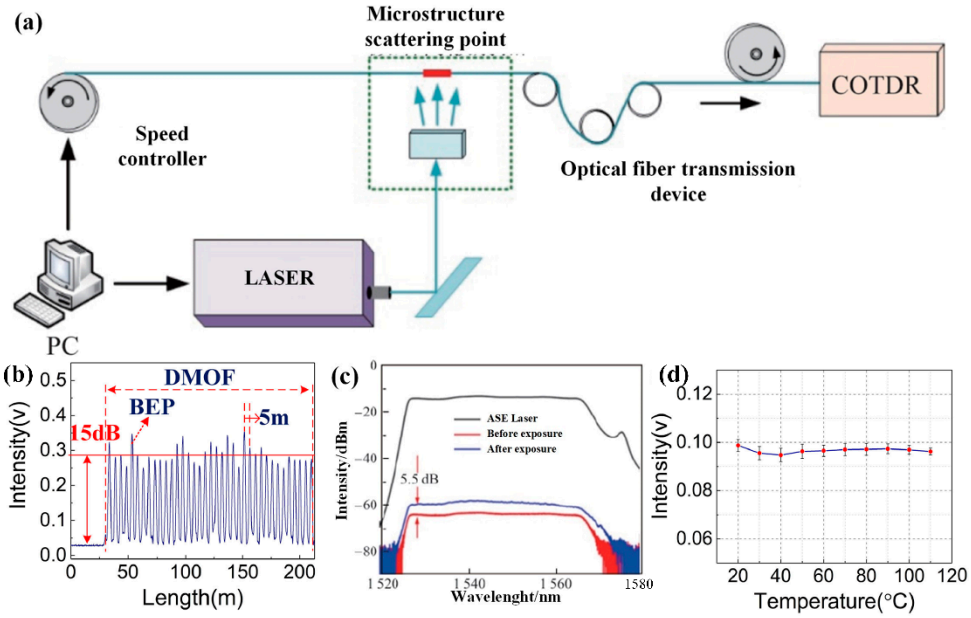

Figure 9. Preparation method for a colorless microstructure array based on UV exposure: (**a**) automatic colorless microstructure preparation system [51]; (**b**) OTDR measurement results of colorless microstructure array [53]; (**c**) spectra of colorless microstructure arrays [51]; (**d**) temperature stability of colorless microstructure arrays [53].

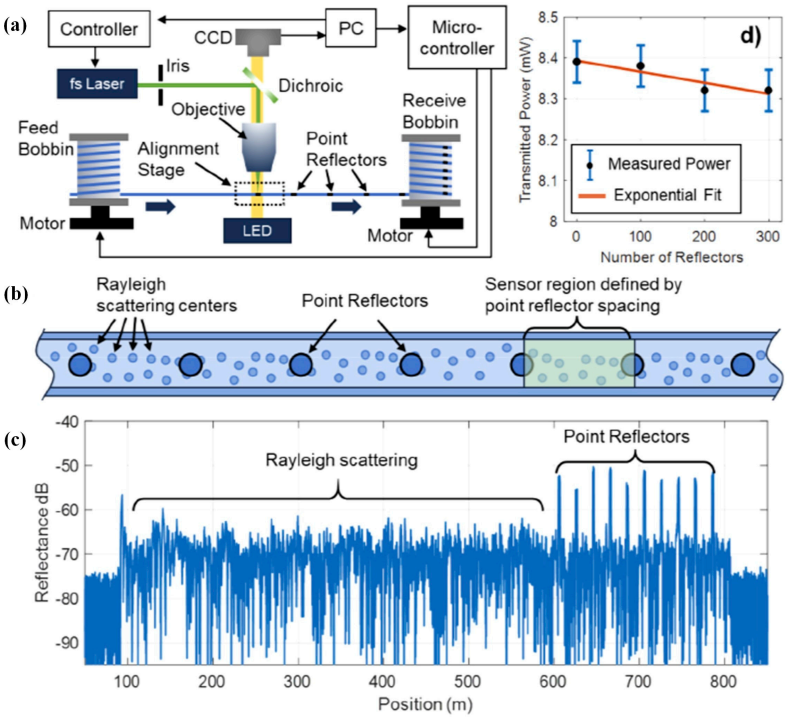

Figure 10. Preparation method for a weak reflection array based on a femtosecond laser [40]: (**a**) weak reflection array preparation system; (**b**) schematic diagram of weak reflection array preparation method; (**c**) OTDR measurement results for the weak reflection array; (**d**) the result of a cut-back measurement on a separate fiber containing 300 reflectors.

3.4. Methods to Improve the Performance of Specialty Fiber DAS

In the early stages, researchers mainly focused on using UWFBG in various DAS schemes. In 2015, Wang et al. used UWFBG in DAS based on a 3 × 3 coupler demodulation for hydroacoustic testing, which can detect a water pressure of 0.112 Pa [55]. Subsequently,

the team at Huazhong University of Science and Technology successively used DSE fiber in various DAS schemes, such as double-pulse, coherent detection, and PGC demodulation schemes [29,39,40,50,56–58]. These schemes are shown in Figure 11. In recent years, more attention has been paid to improving the DAS system performance by using the advantages of discrete scattering enhancement fiber, including low-frequency phase shift compensation, polarization fading suppression, pulse width compression, and system sampling rate expansion.

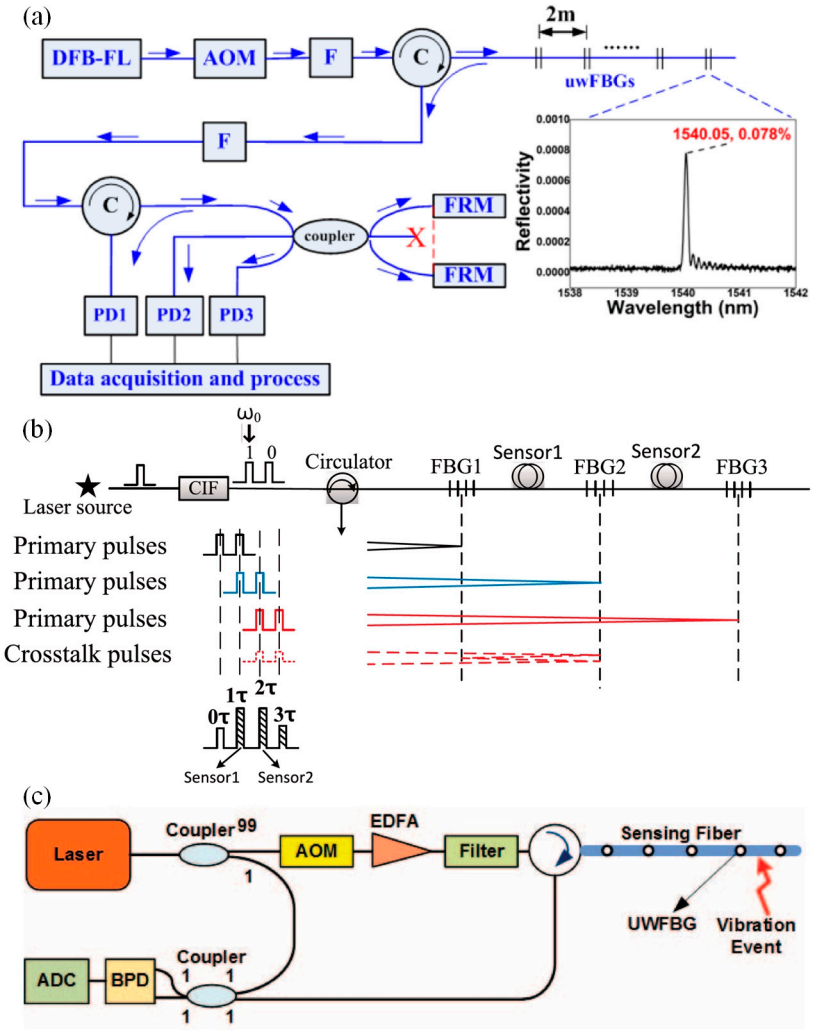

Figure 11. Representative DAS scheme based on UWFBG: (**a**) scheme using a 3 × 3 coupler [54]; (**b**) PGC scheme [55]; (**c**) heterodyne coherent detection scheme [29].

3.4.1. Low-Frequency Phase Drift Compensation Technology

The DSE fiber DAS has the potential for extremely low-frequency detection due to its good signal consistency and lac of interference of random Rayleigh scattering. In the DAS system, the low-frequency drift of the laser phase and the slow change of the external temperature will introduce greater low-frequency noise to the system, limiting the accuracy of the low-frequency detection [59]. The phase drift of the laser can be compensated by the auxiliary interferometer. As shown in Figure 12a, the phase noise of the laser is measured in real time by the auxiliary interferometer, and the measurement results are compensated to suppress the low-frequency noise. In this way, Fan et al. achieved a strain resolution of $3.84 p\varepsilon/\sqrt{\text{Hz}}$ [60,61] at a frequency of 10 Hz. The team from Huazhong University of Science and Technology proposed a reference fiber compensation scheme via the discrete enhancement of UWFBG. The scheme is shown in Figure 12b, which can

compensate for laser drift and temperature changes at the same time, achieving a resolution of $0.57n\varepsilon/\sqrt{Hz}$ at a frequency of 0.01 Hz and a resolution of $3.4n\varepsilon/\sqrt{Hz}$ at a frequency of 10 Hz [62]. Furthermore, the team introduced an LS-SVM operator during demodulation to track and compensate for the hysteresis effect of the temperature, allowing high-precision acoustic measurements in the 0.001 Hz frequency band [63].

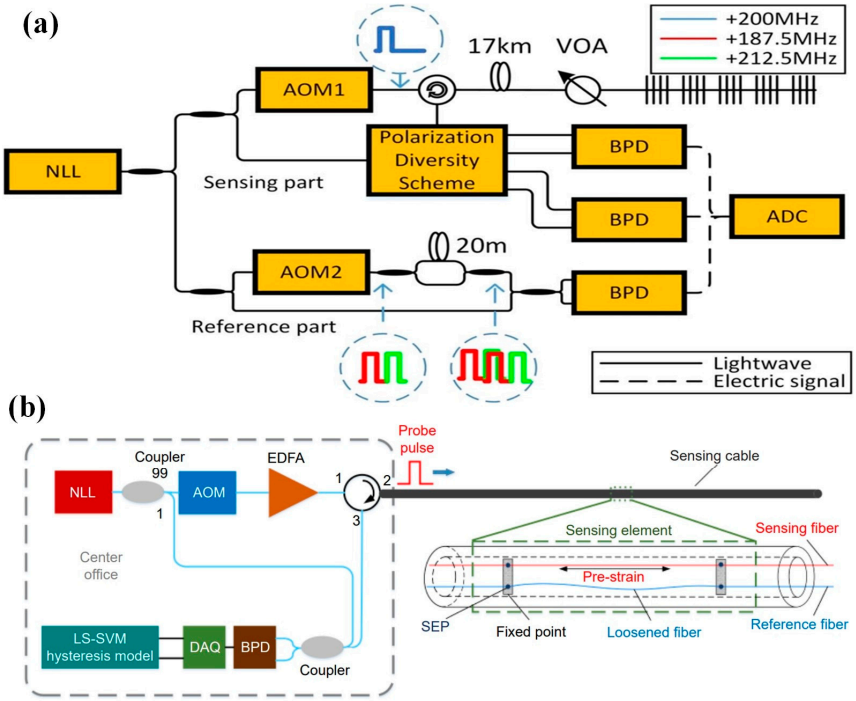

Figure 12. Representative scheme for low-frequency noise suppression: (**a**) auxiliary interferometer compensation [60,61]; (**b**) reference fiber compensation [62].

3.4.2. Polarization Fading Suppression Technology

In the DSE-fiber-based DAS system, the coherent fading is completely suppressed, while the polarization random fading problem must be urgently solved [16]. The random polarization fading is caused by the random change in polarization states of the two interference lights. When the polarization directions of the two interference lights are parallel, the interference light signal is the largest and the phase noise is the smallest. However, when the directions are orthogonal, the interference light intensity is decreased to zero and the phase information is completely overwhelmed by noise. In order to solve this problem, Zhang et al. improved the dual-wavelength DAS scheme. As shown in Figure 13, the polarization composite double pulse was used as the detection pulse to achieve polarization noise suppression [16,64]. For the coherent detection DAS scheme, Sun et al. used a polarization beam splitter to divide the reflected light into two orthogonal polarization states to interfere with the local oscillator light, so that the random polarization noise was reduced by 9.5 dB [65]. However, in this scheme, when the polarization states of the local oscillator light and the polarization beam splitter do not match, fading may still occur. To resolve this problem, the Huazhong University of Science and Technology team proposed a method for emitting dual-wavelength probe pulses and using the random polarization states of different wavelength parameters to greatly reduce the probability of polarization fading and to reduce polarization noise by 19.2 dB [66].

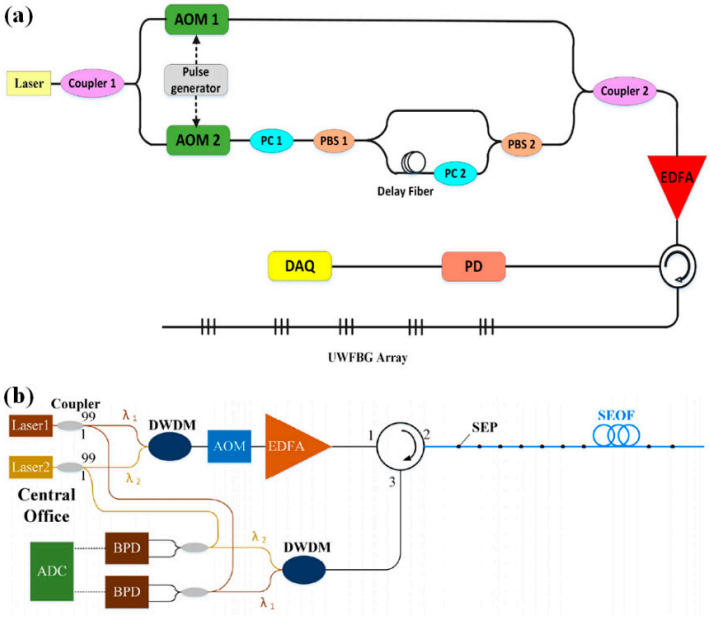

Figure 13. Representative scheme for polarization noise suppression: (**a**) orthogonal polarization scheme [16]; (**b**) multi-parameter scheme [66].

3.4.3. Pulse Width Compression Technology

In the DAS system, the interval between the SEPs determines the resolution of the system and also limits the width of the detection pulse. Assuming that the interval between the SEPs is d, the detection pulse is limited to $\tau \leq 2dn/c$ (where n is the refractive index of the fiber and c is the speed of light in the vacuum). In a radar system, a longer detection pulse is usually transmitted and the pulse is compressed at the receiving end, so as to obtain a signal with a high signal-to-noise ratio under the premise of ensuring the resolution. The common schemes are pulse linear frequency sweeping and pulse coding [67–69]. These techniques have also been used in DSE fiber DAS systems. Fan et al. adopted the sweeping pulse transmission scheme, whereby the receiving end compresses the pulses through matched filtering, achieving a noise level of -93.16dB re rad$/\sqrt{\text{Hz}}$ at 500–2500 Hz as shown in Figure 14a [70,71]. Wang et al. successively used pulse coding technology in UWFBG-based DAS systems and improved the systems' SNR values by 6.9 dB as shown in Figure 14b [72].

3.4.4. Sampling Frequency Expansion Technology

In DAS system, the sampling rate is mainly limited by the length of the sensing fiber. After the system transmits the probe pulse into the optical fiber, it needs to ensure that the Rayleigh backscattering signal transmitted to the farthest end of the pulse returns to the receiving end before transmitting the next pulse, otherwise crosstalk will occur. However, during railway safety detection and power grid partial discharge detection applications, it is necessary for the DAS system to perform long-distance and high-frequency detection simultaneously. The way to solve these problems is to transmit multiple probe lights in parallel and distinguish them through a certain feature to avoid crosstalk. By transmitting pulses with different frequencies into the optical fiber and distinguishing them by using different pulse frequencies, Zhang et al. achieved a sampling rate of 440 kHz on a 330 m optical fiber and expanded the distance bandwidth product by three times [73]. Sun et al. put forward a time slot multiplexing scheme. As shown in Figure 15, multiple pulses are inserted into the time slot between two adjacent SEPs of an optical fiber, with a sampling rate of 300 kHz being achieved on a 1020 m optical fiber, expanding the distance bandwidth product by six times [74].

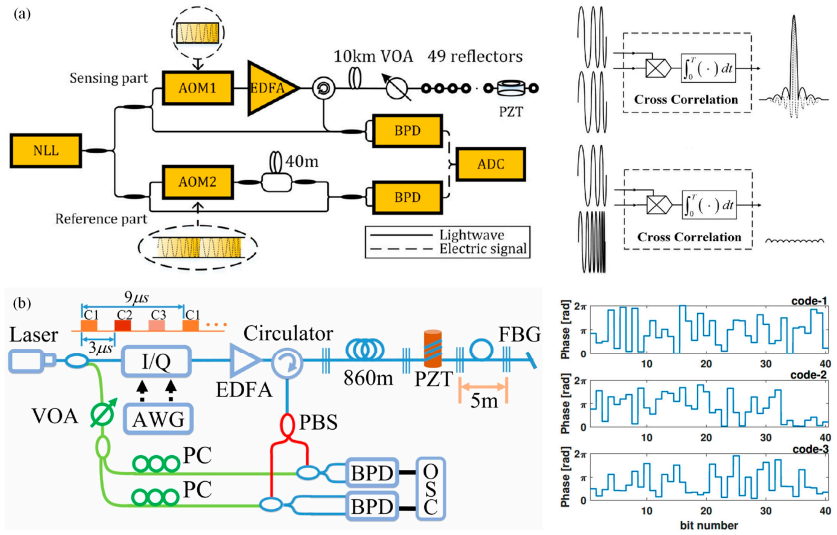

Figure 14. Representative scheme for pulse width compression: (**a**) orthogonal polarization scheme [70,71]; (**b**) multi-parameter scheme [72].

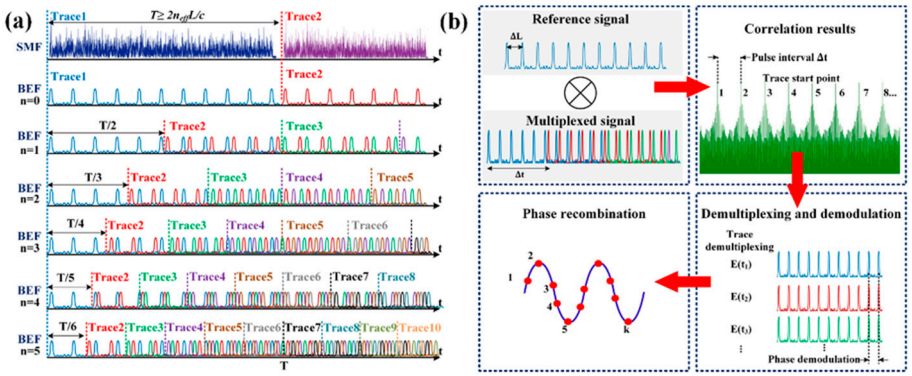

Figure 15. Time slot multiplexing scheme [74]: (**a**) principle; (**b**) demodulation algorithm.

Above, the two specialty fibers, namely CSE fiber and DSE fiber, are analyzed and compared in terms of SNR enhancements, sensing distance, and methods to improve the performance. As shown in the Table 2, it can be seen that the DSE fiber performs significantly better than the CSE fiber in terms of the sensing distance, while the greater number of matching DAS schemes also further improves the performance of DAS system in multiple dimensions.

Table 2. Performance summary for CSE and DSE fibers.

	Fabrication Method	SNR Enhancements	Sensing Distance
CSE fiber	Continuously inscribe Bragg gratings [31–34]	15 dB [31]	1 km [31]
	Highly doped fiber [35,36]	14 dB [36]	1.9 km [36]
DSE fiber	UV exposure [41–43,47,51–53]	5.5–21.1 dB [41–43,47,51]	50 km [51]
	Femtosecond laser inscription [40,44,45,54]	13–15.8 dB [40,54]	9.8 km [54]

4. Significant Application Progress

With the continuous improvement and development of the DAS system based on the specialty scattering-enhanced optical fiber, researchers have applied the system to practical engineering applications in many fields, including geological and resource exploration, structural health monitoring, and hydroacoustic exploration.

4.1. Geological and Resource Exploration

The vertical seismic profile (VSP) is a commonly used parameter for petroleum exploration seismic observations. With the development of DAS technology, fiberoptic logging has become a research hotspot.

Sun et al. conducted a walkaway VSP experiment using a self-made microstructure fiber DAS system [75]. The microstructure fiber is arranged vertically in the test well and the explosive source is artificially introduced on the ground to generate seismic waves, which are transmitted along the stratum to generate direct waves and reflected waves. Figure 16 shows the VSP results recorded at the "zero bias" position and 2.5 km away from the "non-zero bias" position. Figure 16a is the seismic wave transmission diagram recorded by the microstructure fiber DAS system under the condition of "zero bias". The specific details are enlarged, as shown in Figure 16b. It can be observed that clear direct transmission of the p-wave and s-wave is demonstrated, and that the peaks and troughs of multi-channel signals correspond to each other, highlighting the phase difference caused by the transmission time, which proves the high consistency of the microstructure fiber DAS system. In addition, as shown in Figure 16c, for the "non-zero biased" signal away from 2.5 km, the microstructure fiber DAS can also record direct waves and reflected waves with high SNR values. The DAS system based on microstructure fiber has the advantages of a high SNR, high signal consistency, and high reliability, meaning it could become an efficient, fast, and reliable acquisition tool for oil data acquisition, potentially allowing intelligent resource exploration.

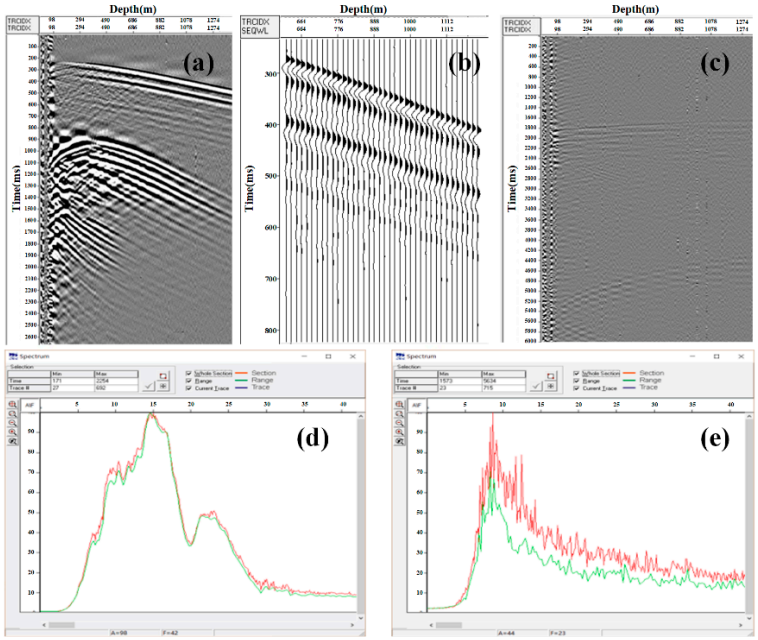

Figure 16. VSP test results for the microstructure fiber DAS system [75]: (**a**) "zero bias" test results; (**b**) schematic diagram of signal consistency; (**c**) "non-zero bias" test results; (**d**) "zero bias" spectrum diagram; (**e**) "non-zero bias" spectrum.

In 2019, Yang built a DAS system based on a UWFBG array [76], using UWFBG to enhance the intensity of the fiber's backscattered signal as shown in Figure 17. In the experiment, the results measured by optical fiber were compared with the waveforms measured

by geophone, and the time-frequency results were in good agreement. Furthermore, it was applied to VSP logging, and a clear VSP waveform with a high SNR was obtained without any data processing.

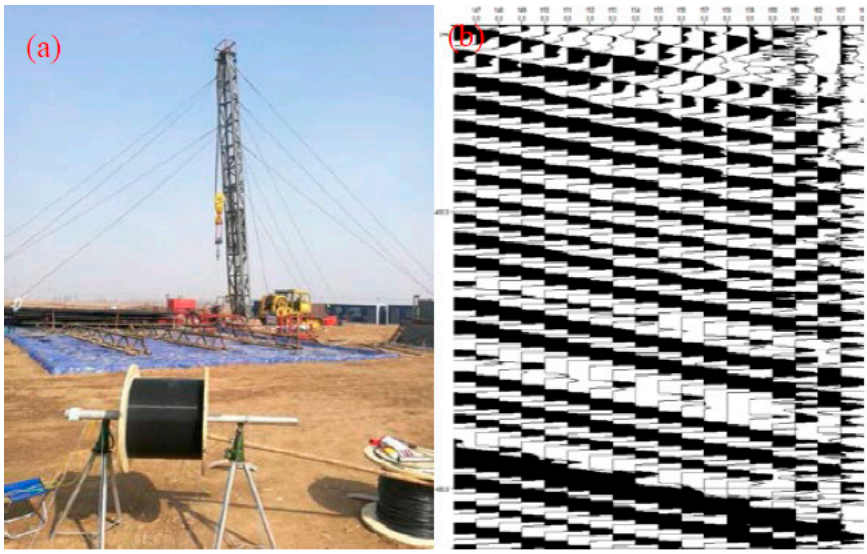

Figure 17. (**a**) The VSP test site. (**b**) The VSP test result [76].

4.2. Structural Health Monitoring

The health status of various infrastructure, such as railways, tunnels, and pipelines, is related to operational safety, the national economy, and social production. The DAS system based on scattering-enhanced fibers was applied to the field of structural health monitoring to ensure high reliability.

4.2.1. Pipeline Monitoring

The transportation of resources such as oil and natural gas is closely related to the national economy and people's lives, but transmission pipelines may fail due to external invasion, corrosion, and other reasons, threatening the safety of personal, profits, and property. The DAS system based on discrete enhanced optical fibers was applied for pipeline safety monitoring due to its high SNR and high stability [77,78].

A team from the University of Pittsburgh [79] used femtosecond writing technology to artificially introduce optical fiber SEPs. As shown in Figure 18, the high-SNR DAS system tracks the propagation characteristics of soundwaves in the pipeline, combined with neural-network-based machine learning algorithms, and the data collected by the DAS system are analyzed to identify external intrusion events and the internal corrosion status of the pipeline. The system's recognition accuracy for different external intrusion events exceeds 85%, the defect recognition accuracy rate exceeds 94% under supervised learning conditions, while the recognition accuracy rate reaches 71% under unsupervised learning conditions. Furthermore, the team also conducted a test of the sand content and the solid–liquid two-phase flow of the pipeline by laying a discrete scattering enhancement fiber on the pipeline wall. By tracking the acoustic emission signals induced by the sand particles in the liquid hitting the pipe wall, the measurement of different sand particle concentrations was achieved.

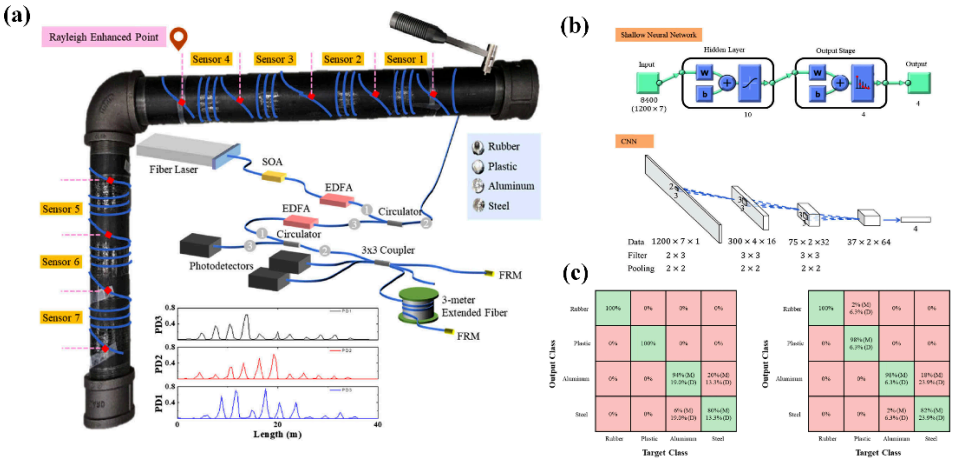

Figure 18. Schematic diagram of a pipeline survey [79]: (**a**) schematic diagram of DAS system for pipeline protection; (**b**) architectures of neural networks in the pipeline protection system; (**c**) the confusion matrix of four acoustic events.

4.2.2. Track Defect Monitoring

With the development of high-speed railway technology, track defect monitoring has become more important. A variety of mature detection methods have been developed, but most of them involve electromagnetic sensors, which are vulnerable to harsh environments [80]. In 2019, Sun et al. used a DAS system based on scattering-enhanced fibers for distributed detection of a railway defect [81]. As shown in Figure 19, the scattering-enhanced fiber is set in the middle of the rail. At the position where the defect occurs, the interaction between the wheel and rail will form an impact sound signal, which is transmitted along the two directions of the track. The DAS system is used to track the transmission signal, and then the accurate positioning of the defect is identified through the positioning algorithm, the results of which show that the maximum error of the defect is only 2.1 m. This method can provide an effective and reliable solution for rail health monitoring.

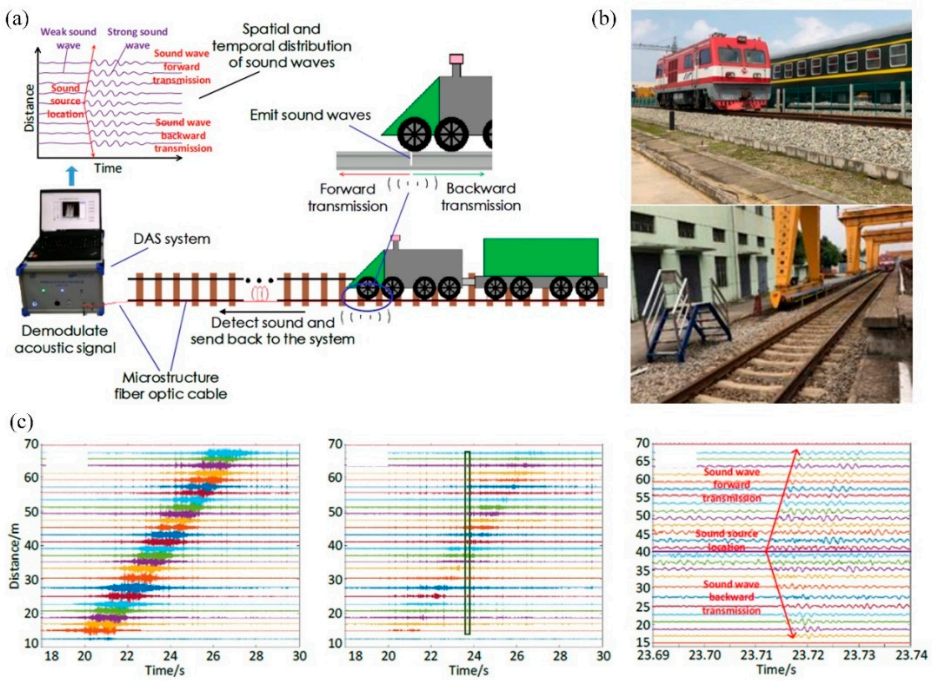

Figure 19. Rail defect detection based on DAS system [80]: (**a**) the process of detecting and analyzing sound waves based on fiber DAS; (**b**) photographs of the field test environment; (**c**) sound distribution measured by DAS.

4.2.3. Tunnel Safety Monitoring

In addition, the health of infrastructure such as tunnels is related to the traffic operation safety. An optical fiber DAS system can also be used for safety detection in tunnels, such as in subways and highways. However, the effectiveness of the reinforcement segment and steel loop in the tunnel structure maybe be a problem. The partial separation of the segment and steel loop will mean the steel loop is unable to effectively support the segment, resulting in potential safety hazards. A resonant cavity will be formed between the segment and the steel loop due to the separation, with different degrees of invalidity corresponding to the different resonant frequencies. In 2021, Sun et al. carried out intelligent monitoring of a tunnel steel loop structure based on a scattering-enhanced optical fiber DAS system [81]. As shown in Figure 20, the sensing fiber is laid on the steel loop structure to obtain the resonant frequency changes induced by the active sound source. Furthermore, the machine learning algorithm based on the BP neural network is used to effectively classify different failure levels, so as to achieve the online detection of the bonding state of the reinforced steel loop. The experimental results show that the system has a recognition rate of up to 97.8%.

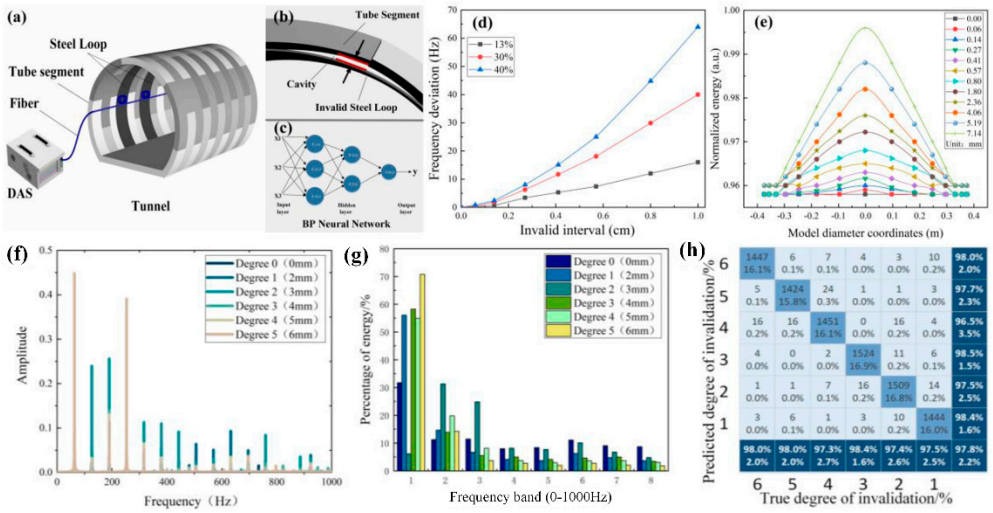

Figure 20. (**a**) Tunnel steel loop detection system based on DAS. (**b**) Schematic diagram of an invalid steel loop. (**c**) BP neural network. (**d**) Relationship between the degree of invalidity and the frequency deviation, (**e**) Relationship between the degree of invalidity and the energy distribution. (**f**) Power spectrum under different degrees of invalidity. (**g**) Wavelet energy transformation under different degrees of invalidity. (**h**) Recognition rate [81].

4.2.4. Geological Structural Monitoring

In recent years, DAS monitoring has been used for geological structures [82]. In 2017, a team from the University of California Berkeley transformed fiberoptic telecommunication cables into sensor arrays enabling meter-scale recording over tens of kilometers of linear fiber length to record the nearly vertically incident arrival of an earthquake from the Geysers Geothermal Field and to estimate its backazimuth and speed [83]. In 2018, Jousset et al. demonstrated the possibility of dynamic strain determination with conventional fiber cables deployed for telecommunication [84]. Then, by using DAS, they recorded seismic signals from natural and man-made sources with 4 m spacing along a 15-km-long fiber cable, identifying new dynamic fault processes with unprecedented resolution, opening a new path for earth hazard assessments and the exploration of structural features. In 2019, Sladen et al. reported measurements on a 41.5-km-long telecom cable that was deployed offshore of Toulon, France, demonstrating the capability to monitor the ocean's solid earth interactions from the coast to the abyssal plain [85]. In the same year, Lindsey et al. reported the use of an optical fiber cable with a DAS operating onshore, creating a ~10,000-component, 20-km-long seismic array. As depicted in Figure 21, they recorded

a minor earthquake wavefield, identified multiple submarine fault zones, and tracked sea-state dynamics during a storm cycle in the northern Pacific Ocean [86].

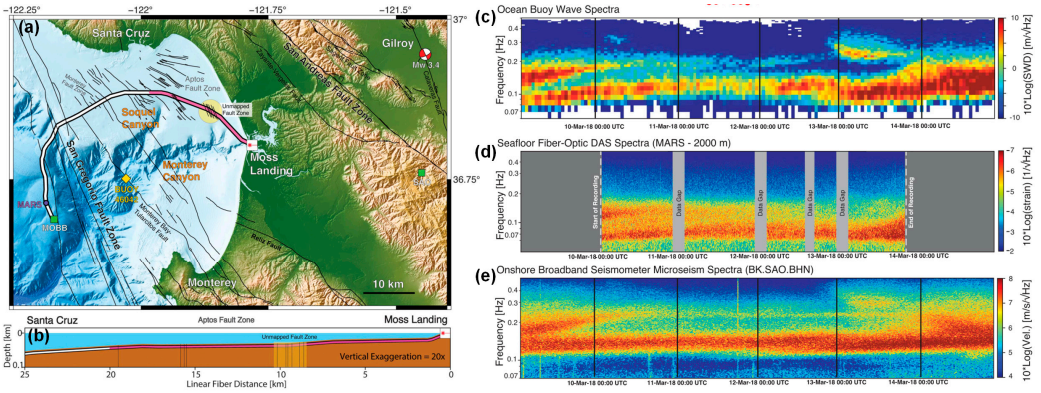

Figure 21. (**a**) Map of Monterey Bay, CA, showing the Monterey Accelerated Research System (MARS) cable (DAS, pink portion), mapped faults, the Gilroy earthquake (red and white beach ball), and major bathymetric features. (**b**) Cross-section illustration of the MARS cable used for DAS. (**c**) The 10 min average wave height and spectral wave density (SWD) measurements outside Monterey Bay, which were measured using a buoy. (**d**) Seafloor DAS strain from a 2 km cable location averaged over a 15 min sliding window. (**e**) North component of ground velocity from an onshore broadband inertial seismometer averaged over a 15 min sliding window [86].

4.3. Hydroacoustic Exploration

Ocean exploration is of great significance to homeland security and resource exploration. The acoustic medium can carry a wealth of information and can transmit signals for long distances underwater, so hydrophones are an important tool for underwater information acquisition. Optical fiber sensors have been preliminarily used in the field of underwater acoustic measurement due to their unique advantages. Single-point sensors and hydrophone arrays based on FBG and interferometers were common methods used for early optical fiber hydrophones. However, due to the limited multiplexing capacity, it is difficult to meet the requirements for large-scale exploration in the ocean and other application environments. In recent years, the DAS system has been well applied in the field of terrestrial acoustic detection. Because of its distributed, long-distance, and high-sensitivity characteristics, the DAS system has been introduced into the field of hydrophones. In the preliminary stage, researchers measured the underwater acoustic sensitivity and other parameters of an optical fiber in the laboratory. Usually, a distributed underwater acoustic sensing system is built based on a UWFBG array and unbalanced interferometer demodulation structure [54,87]. The underwater acoustic signal is obtained by demodulating the change in phase difference between two adjacent UWFBGs, in which the sensitivity obtained usually reaches about −160~−150 dB re rad/μPa.

In 2021, Sun et al. designed a lightweight and fully distributed hydroacoustic optical sensing cable [88]. An acoustic sensitizing layer is superimposed on the inner core layer, the microstructure scattering-enhanced fiber is wound on the sensitizing layer, and a further protective layer is added to the outermost layer. As depicted in Figure 22, the coherent detection system has been utilized to conduct experiments, with the results showing that the hydroacoustic detection sensitivity is as high as −127 dB re rad/μPa with a flat frequency response range of 100–2000 Hz. Furthermore, the team conducted an on-site lake test, the results of which are depicted in Figure 23.

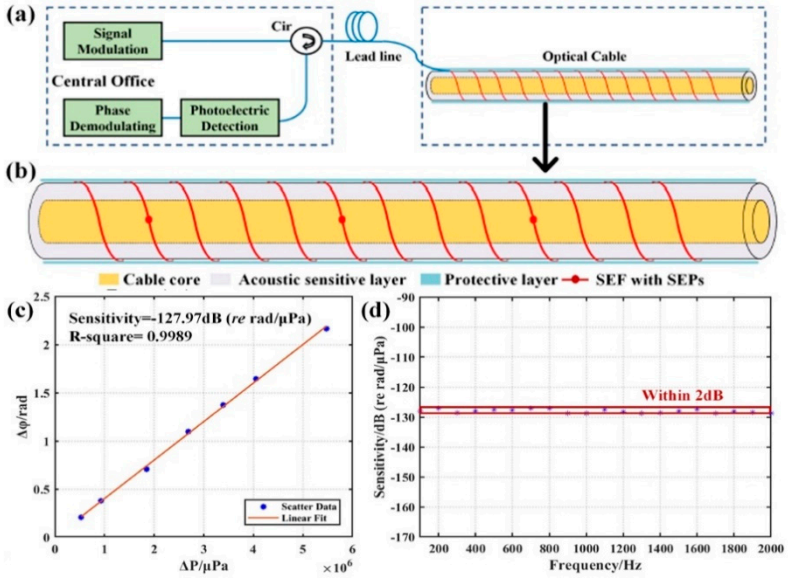

Figure 22. (**a**) Fully distributed underwater acoustic sensor system. (**b**) Lightweight fully distributed underwater acoustic fiberoptic cable based on scattering-enhanced fiber. (**c**) The relationship between the phase demodulation change and acoustic pressure. (**d**) The frequency response curve within the frequency range of 100–2000 Hz [88].

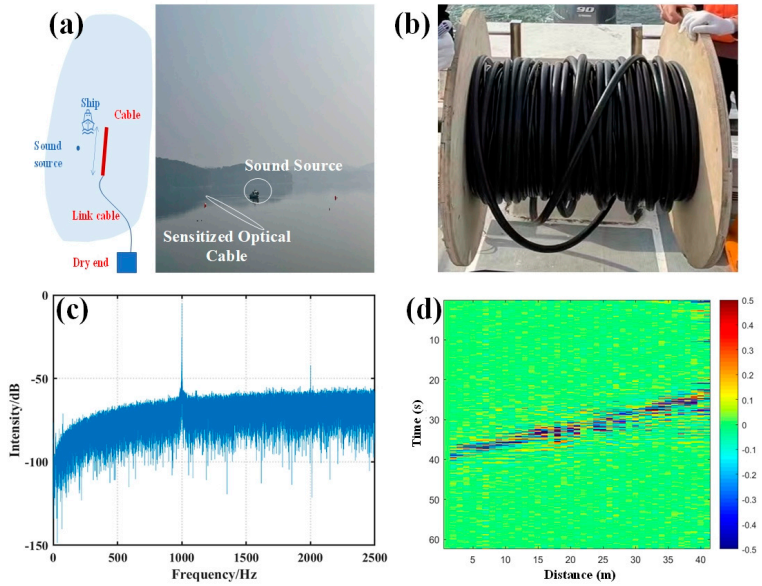

Figure 23. The underwater acoustic test: (**a**) the setup for the field test; (**b**) picture of the sensitized optical cable; (**c**) the static test results for the sound source; (**d**) motion trajectory tracking of the sound source.

5. Conclusions and Prospects

The variability and functionality of specialty optical fibers have demonstrated their major potential for sensing performance enhancement and application development for DAS systems. In this review, the scattering characteristics and noise suppression principles of specialty optical fibers are analyzed, and the fabrication technologies used for DSE are introduced. Based on the discrete scattering-enhanced fiber, the performance enhancement technologies of the DAS system are summarized, including the low-frequency phase noise compensation, polarization fading suppression, pulse width compression, and system sampling rate expansion. Further, due to the unique advantages of the scattering-enhanced fiber, the DAS system has been widely applied in various fields, such as in resource

exploration, structural health monitoring, and for distributed hydrophones. Looking to the future, the research on the specialty-fiber based DAS will develop rapidly for many aspects, such as the doping of new materials for high sensitization, the development of fabrication techniques for higher efficiency, the introduction of AI techniques for higher measurement accuracy, and the exploration of wider application fields. Owing to the distinct advantages, it is believed that the specialty-fiber-based DAS system will have bright market prospects in geological, resource, and hydroacoustic exploration, as well as structural health monitoring.

Author Contributions: Conceptualization, Q.S. and Z.Y.; methodology, H.L. and C.F.; formal analysis, Y.S. and J.C.; investigation, B.Y.; writing—original draft preparation, Y.S.; writing—review and editing, Y.S.; funding acquisition, Q.S. All authors have read and agreed to the published version of the manuscript.

Funding: This research was supported by National Natural Science Foundation for Distinguished Young Scholars through Grant No. 61922033; the Marine economic development project of Guangdong Province through Grant No. GDNRC 2020(045); the National Natural Science Foundation of China through Grant No. 61775072; and the Innovation Fund of WNLO.

Institutional Review Board Statement: Not applicable.

Informed Consent Statement: Not applicable.

Data Availability Statement: Not applicable.

Conflicts of Interest: The authors declare no conflict of interest.

References

1. Yatman, G.; Üzumcü, S.; Pahsa, A.; Mert, A.A. Intrusion detection sensors used by electronic security systems for critical facilities and infrastructures: A review. *Safe* **2015**, *151*, 131–141. [CrossRef]
2. Shelef, E.; Oskin, M. Deformation processes adjacent to active faults: Examples from eastern California. *J. Geophys. Res. Earth Surf.* **2010**, *115*. [CrossRef]
3. Mu, D.; Lee, E.J.; Chen, P. *Seismic Imaging, Fault Damage and Heal*; De Gruyter: Berlin, Germany, 2014; ISBN 9787040390988.
4. Thun, J.; Lokmer, I.; Bean, C.; Eibl, E.; Bergsson, B.H.; Braiden, A. Micrometre-scale deformation observations reveal fundamental controls on geological rifting. *Sci. Rep.* **2016**, *6*, 36676. [CrossRef] [PubMed]
5. Hartog, A.; Frignet, B.; Mackie, D.; Clark, M. Vertical seismic optical profiling on wireline logging cable. *Geophys. Prospect.* **2014**, *62*, 693–701. [CrossRef]
6. Tejedor, J.; Ahlen, C.H.; Gonzalez-Herraez, M.; Macias-Guarasa, J.; Martins, H.F.; Pastor-Graells, J.; Martin-Lopez, S.; Guillen, P.C.; De Pauw, G.; De Smet, F.; et al. Real Field Deployment of a Smart Fiber-Optic Surveillance System for Pipeline Integrity Threat Detection: Architectural Issues and Blind Field Test Results. *J. Light. Technol.* **2017**, *36*, 1052–1062. [CrossRef]
7. Lyu, C.; Huo, Z.; Cheng, X.; Jiang, J.; Alimasi, A.; Liu, H. Distributed Optical Fiber Sensing Intrusion Pattern Recognition Based on GAF and CNN. *J. Light. Technol.* **2020**, *38*, 4174–4182. [CrossRef]
8. Masoudi, A.; Belal, M.; Newson, T.P. A distributed optical fibre dynamic strain sensor based on phase-OTDR. *Meas. Sci. Technol.* **2013**, *24*, 085204. [CrossRef]
9. Zhou, L.; Wang, F.; Wang, X.; Pan, Y.; Sun, Z.; Hua, J.; Zhang, X. Distributed Strain and Vibration Sensing System Based on Phase-Sensitive OTDR. *IEEE Photon. Technol. Lett.* **2015**, *27*, 1884–1887. [CrossRef]
10. Gabai, H.; Eyal, A. On the sensitivity of distributed acoustic sensing. *Opt. Lett.* **2016**, *41*, 5648–5651. [CrossRef]
11. Healey, P. Fading in heterodyne OTDR. *Electron. Lett.* **1984**, *20*, 30–32. [CrossRef]
12. Zabihi, M.; Chen, Y.; Zhou, T.; Liu, J.; Shan, Y.; Meng, Z.; Wang, F.; Zhang, Y.; Zhang, X.; Chen, M. Continuous Fading Suppression Method for Φ-OTDR Systems Using Optimum Tracking Over Multiple Probe Frequencies. *J. Light. Technol.* **2019**, *37*, 3602–3610. [CrossRef]
13. Zhou, J.; Pan, Z.; Ye, Q.; Cai, H.; Qu, R.; Fang, Z. Characteristics and Explanations of Interference Fading of a Φ-OTDR With a Multi-Frequency Source. *J. Light. Technol.* **2013**, *31*, 2947–2954. [CrossRef]
14. Ren, M.; Lu, P.; Chen, L.; Bao, X. Theoretical and Experimental Analysis of O-OTDR Based on Polarization Diversity Detection. *IEEE Photon. Technol. Lett.* **2015**, *28*, 697–700. [CrossRef]
15. Mompo, J.J.; Shiloh, L.; Arbel, N.; Levanon, N.; Loayssa, A.; Eyal, A. Distributed Dynamic Strain Sensing via Perfect Periodic Coherent Codes and a Polarization Diversity Receiver. *J. Light. Technol.* **2019**, *37*, 4597–4602. [CrossRef]
16. Wang, F.; Liu, Y.; Wei, T.; Zhang, Y.; Ji, W.; Zong, M.; Zhang, X. Polarization fading elimination for ultra-weak FBG array-based Φ-OTDR using a composite double probe pulse approach. *Opt. Express* **2019**, *27*, 20468–20478. [CrossRef]
17. Qin, Z.; Zhu, T.; Chen, L.; Bao, X. High Sensitivity Distributed Vibration Sensor Based on Polarization-Maintaining Configurations of Phase-OTDR. *IEEE Photon. Technol. Lett.* **2011**, *23*, 1091–1093. [CrossRef]

18. He, X.; Zhang, M.; Gu, L.; Xie, S.; Liu, F.; Lu, H. Performance Improvement of Dual-Pulse Heterodyne Distributed Acoustic Sensor for Sound Detection. *Sensors* **2020**, *20*, 999. [CrossRef]
19. Juarez, J.C.; Maier, E.W.; Choi, K.N.; Taylor, H.F. Distributed fiber-optic intrusion sensor system. *J. Lightwave Technol.* **2005**, *23*, 2081–2087. [CrossRef]
20. Rao, Y.-J.; Luo, J.; Ran, Z.-L.; Yue, J.-F.; Luo, X.-D.; Zhou, Z. Long-distance fiber-optic Φ-OTDR intrusion sensing system. In Proceedings of the Spie the International Society for Optical Engineering, San Diego, CA, USA, 3–4 August 2009; Volume 7503, p. 75031O. [CrossRef]
21. Juarez, J.C.; Taylor, H.F. Polarization discrimination in a phase-sensitive optical time-domain reflectometer intrusion-sensor system. *Opt. Lett.* **2005**, *30*, 3284–3286. [CrossRef]
22. Pan, Z.; Liang, K.; Ye, Q.; Cai, H.; Qu, R.; Fa Ng, Z. Phase-sensitive OTDR system based on digital coherent detection. In Proceedings of the SPIE Proceedings (SPIE SPIE/OSA/IEEE Asia Communications and Photonics-Shanghai, China), Shanghai China, 13–16 November 2011; Volume 8311, p. 83110S-2. [CrossRef]
23. Zhang, X.; Sun, Z.; Shan, Y.; Li, Y.; Wang, F.; Zeng, J.; Zhang, Y. A high performance distributed optical fiber sensor based on Φ-OTDR for dynamic strain measurement. *IEEE Photon. J.* **2017**, *9*, 1–12. [CrossRef]
24. Fang, G.; Xu, T.; Feng, S.; Li, F. Phase-Sensitive Optical Time Domain Reflectometer Based on Phase-Generated Carrier Algorithm. *J. Light. Technol.* **2015**, *33*, 2811–2816. [CrossRef]
25. Chen, D.; Liu, Q.; Fan, X.; He, Z. Distributed Fiber-Optic Acoustic Sensor with Enhanced Response Bandwidth and High Signal-to-Noise Ratio. *J. Light. Technol.* **2017**, *35*, 2037–2043. [CrossRef]
26. Liokumovich, L.; Ushakov, N.; Kotov, O.; Bisyarin, M.; Hartog, A.H. Fundamentals of Optical Fiber Sensing Schemes Based on Coherent Optical Time Domain Reflectometry: Signal Model Under Static Fiber Conditions. *J. Light. Technol.* **2015**, *33*, 3660–3671. [CrossRef]
27. Zhang, J.; Wu, H.; Zheng, H.; Huang, J.; Yin, G.; Zhu, T.; Qiu, F.; Huang, X.; Qu, D.; Bai, Y.; et al. 80 km Fading Free Phase-Sensitive Reflectometry Based on Multi-Carrier NLFM Pulse Without Distributed Amplification. *J. Light. Technol.* **2019**, *37*, 4748–4754. [CrossRef]
28. Li, H.; Liu, Y.; He, T.; Fan, C.; Liu, T.; Yan, Z.; Liu, D.; Sun, Q. Dual-pulse Complex Superposition Based Noise Suppression for Distributed Acoustic Sensing. In Proceedings of the CLEO: Applications and Technology, Washington, DC, USA, 10–15 May 2020; p. JW2E.28. [CrossRef]
29. Ai, F.; Sun, Q.; Zhang, W.; Liu, T.; Yan, Z.; Liu, D. Wideband Fully-Distributed Vibration Sensing by Using UWFBG Based Coherent OTDR. In Proceedings of the Optical Fiber Communications Conference & Exhibition, Los Angeles, CA, USA, 19–23 March 2017; p. W2A.19. [CrossRef]
30. Lin, S.T.; Wang, Z.N.; Xiong, J.; Wu, Y.; Rao, Y.J. Progresses of Anti-Interference-Fading Technologies for Ray-leigh-Scattering-Based Optical Fiber Sensing. *Laser Optoelectron. Prog.* **2021**, *58*, 1306008. [CrossRef]
31. Westbrook, P.S.; Feder, K.S.; Ortiz, R.M.; Kremp, T.; Monberg, E.M.; Wu, H.; Simoff, D.A.; Shenk, S. Kilometer length low loss enhanced back scattering fiber for distributed sensing. In Proceedings of the 25th International Conference on Optical Fiber Sensors, Jeju, Korea, 24–28 April 2017; pp. 1–5. [CrossRef]
32. Handerek, V.A.; Karimi, M.; Nkansah, A.; Yau, A.; Westbrook, P.S.; Feder, K.S.; Ortiz, R.M.; Kremp, T.; Monberg, E.M.; Wu, H.; et al. Improved Optical Power Budget in Distributed Acoustic Sensing Using Enhanced Scattering Optical Fibre. In Proceedings of the 26th International Conference on Optical Fiber Sensors, Vaud, Switzerland, 24–28 September 2018; p. TuC5. [CrossRef]
33. Westbrook, P.S.; Kremp, T.; Feder, K.S.; Ko, W.; Monberg, E.M.; Wu, H.; Simoff, D.A.; Ortiz, R.M. Improving distributed sensing with continuous gratings in single and multi-core fibers. In Proceedings of the Optical Fiber Communication Conference, San Diego, CA, USA, 11–15 March 2018; p. W1K.1. [CrossRef]
34. Lalam, N.; Westbrook, P.S.; Li, J.; Lu, P.; Buric, M.P. Phase-Sensitive Optical Time Domain Reflectometry with Rayleigh Enhanced Optical Fiber. *IEEE Access* **2021**, *9*, 114428–114434. [CrossRef]
35. Butov, O.V.; Chamorovskii, Y.K.; Golant, K.M.; Fotiadi, A.A.; Jason, J.; Popov, S.M.; Wuilpart, M. Sensitivity of high Rayleigh scattering fiber in acoustic/vibration sensing using phase-OTDR. In Proceedings of the Optical Sensing and Detection V, Strasbourg, France, 9 May 2018. [CrossRef]
36. Feng, S.; Xu, T.; Huang, J.; Yang, Y.; Li, F.; Zhou, J.; Yu, H. Enhanced SNR phase-sensitive OTDR system with active fiber. In Proceedings of the Fiber Optic Sensing and Optical Communication, Beijing, China, 12 December 2018. [CrossRef]
37. Huang, J.B.; Ding, P.; Tang, J.S. Progress in Fabrication, Demodulation and Application of Weak-Reflection Fiber Bragg Grating Array. *Laser Optoelectron. Prog.* **2021**, *58*, 1700005. [CrossRef]
38. Wu, M.; Fan, X.; Zhang, X.; Yan, L.; He, Z. Frequency Response Enhancement of Phase-Sensitive OTDR for Interrogating Weak Reflector Array by Using OFDM and Vernier Effect. *J. Light. Technol.* **2020**, *38*, 4874–4882. [CrossRef]
39. Hicke, K.; Eisermann, R.; Chruscicki, S. Enhanced Distributed Fiber Optic Vibration Sensing and Simultaneous Temperature Gradient Sensing Using Traditional C-OTDR and Structured Fiber with Scattering Dots. *Sensors* **2019**, *19*, 4114. [CrossRef]
40. Redding, B.; Murray, M.J.; Donko, A.; Beresna, M.; Masoudi, A.; Brambilla, G. Low-noise distributed acoustic sensing using enhanced backscattering fiber with ultra-low-loss point reflectors. *Opt. Express* **2020**, *28*, 14638–14647. [CrossRef]
41. Hill, K.O.; Fujii, Y.; Johnson, D.C.; Kawasaki, B.S. Photosensitivity in optical fiber waveguides: Application to reflection filter fabrication. *Appl. Phys. Lett.* **1978**, *32*, 647–649. [CrossRef]

42. Meltz, G.; Morey, W.W.; Glenn, W.H. Formation of Bragg gratings in optical fibers by a transverse holographic method. *Opt. Lett.* **1989**, *14*, 823–825. [CrossRef] [PubMed]
43. Zheng, Y.; Yu, H.; Guo, H.; Li, X.; Jiang, D. Analysis of the Spectrum Distortions of Weak Fiber Bragg Gratings Fabricated In-Line on a Draw Tower by the Phase Mask Technique. *J. Light. Technol.* **2014**, *33*, 2670–2673. [CrossRef]
44. Martinez, A.; Dubov, M.; Khrushchev, I.; Bennion, I. Direct writing of fibre Bragg gratings by femtosecond laser. *Electron. Lett.* **2004**, *40*, 1170–1172. [CrossRef]
45. Chen, Z.; He, J.; Xu, X.; He, J.; Xu, B.; Du, B.; Liao, C.; Wang, Y. High-Temperature Sensor Array Based on Fiber Bragg Gratings Fabricated by Femtosecond Laser Point-by-Point Method. *Acta Opt. Sin.* **2021**, *41*, 1306002. [CrossRef]
46. Yang, M.; Bai, W.; Guo, H.; Wen, H.; Yu, H.; Jiang, D. Huge capacity fiber-optic sensing network based on ultra-weak draw tower gratings. *Photon. Sens.* **2016**, *6*, 26–41. [CrossRef]
47. Tang, J.; Cai, L.; Li, C.; Yang, M.; Guo, H.; Gan, W. Distributed acoustic sensors with wide frequency response based on UWFBG array utilizing dual-pulse detection. *Opt. Fiber Technol.* **2021**, *61*, 102452. [CrossRef]
48. Ai, F.; Li, H.; He, T.; Yan, Z.; Liu, D.; Sun, Q. Simultaneous Distributed Temperature and Vibration Measurement with UWFBG based Coherent OTDR. In Proceedings of the Optical Fiber Communication Conference, San Diego, CA, USA, 11–15 March 2018; p. W2A.12. [CrossRef]
49. Yang, M.; Li, C.; Mei, Z.; Tang, J.; Guo, H.; Jiang, D. Thousand of fiber grating sensor array based on draw tower: A new platform for fiber-optic sensing. In Proceedings of the Optical Fiber Sensors, OFS 2018, Lausanne, Switzerland, 24–28 September 2018; p. FB6. [CrossRef]
50. Peng, Z.; Jian, J.; Wen, H.; Wang, M.; Liu, H.; Jiang, D.; Mao, Z.; Chen, K.P. Fiber-optical distributed acoustic sensing signal enhancements using ultrafast laser and artificial intelligence for human movement detection and pipeline monitoring. *Opt. Data Sci. II* **2019**, *10937*, 109370J. [CrossRef]
51. Liu, D.M.; He, T.; Xu, Z.J.; Sun, Q. New type of microstructure-fiber distributed acoustic sensing technology and its applications. *J. Appl. Sci.* **2020**, *38*, 296–309. [CrossRef]
52. Ai, F. Investigation on Discrete Enhanced Fiber Based Distributed Sensing Technologies and Their Applications. Ph.D. Thesis, Huazhong University of Science and Technology, Wuhan, China, 2019.
53. Li, H.; Sun, Q.; Liu, T.; Fan, C.; He, T.; Yan, Z.; Liu, D.; Shum, P.P. Ultra-High Sensitive Quasi-Distributed Acoustic Sensor Based on Coherent OTDR and Cylindrical Transducer. *J. Light. Technol.* **2019**, *38*, 929–938. [CrossRef]
54. Wu, M.; Li, C.; Fan, X.; Liao, C.; He, Z. Large-scale multiplexed weak reflector array fabricated with a femtosecond laser for a fiber-optic quasi-distributed acoustic sensing system. *Opt. Lett.* **2020**, *45*, 3685. [CrossRef] [PubMed]
55. Wang, C.; Shang, Y.; Liu, X.-H.; Wang, C.; Yu, H.-H.; Jiang, D.-S.; Peng, G.-D. Distributed OTDR-interferometric sensing network with identical ultra-weak fiber Bragg gratings. *Opt. Express* **2015**, *23*, 29038–29046. [CrossRef] [PubMed]
56. Jiang, P.; Ma, L.; Wang, W.; Hu, Z.; Hu, Y. Crosstalk Reduction and Demodulation Stability Promotion in Inline Fiber Fabry–Pérot Sensor Array Using Phase Generated Carrier Scheme. *J. Light. Technol.* **2015**, *34*, 1006–1014. [CrossRef]
57. Peng, Z.; Wen, H.; Jian, J.; Gribok, A.; Wang, M.; Huang, S.; Liu, H.; Mao, Z.-H.; Chen, K.P. Identifications and classifications of human locomotion using Rayleigh-enhanced distributed fiber acoustic sensors with deep neural networks. *Sci. Rep.* **2020**, *10*, 21014. [CrossRef] [PubMed]
58. Tang, J.; Liu, Y.; Li, C.; Guo, H.; Yang, M. Distributed Vibration Sensing System with High Signal-to-Noise Ratio Based on Ultra-Weak Fiber Bragg Grating. *Acta Opt. Sin.* **2021**, *41*, 1306014. [CrossRef]
59. Fan, X.; Yang, G.; Wang, S.; Liu, Q.; He, Z. Distributed Fiber-Optic Vibration Sensing Based on Phase Extraction from Optical Reflectometry. *J. Light. Technol.* **2016**, *35*, 3281–3288. [CrossRef]
60. Wu, M.; Fan, X.; Liu, Q.; He, Z. Highly sensitive quasi-distributed fiber-optic acoustic sensing system by interrogating a weak reflector array. *Opt. Lett.* **2018**, *43*, 3594–3597. [CrossRef] [PubMed]
61. Wu, M.; Fan, X.; Liu, Q.; He, Z. Quasi-distributed Fiber-optic Acoustic Sensor using Ultra-weak Reflecting Point Array. In Proceedings of the 26th International Conference on Optical Fiber Sensors, Vaud, Switzerland, 24–28 September 2018; p. WF19. [CrossRef]
62. Liu, T.; Li, H.; Ai, F.; Wang, J.; Fan, C.; Luo, Y.; Yan, Z.; Liu, D.; Sun, Q. Ultra-high Resolution Distributed Strain Sensing based on Phase-OTDR. In Proceedings of the Optical Fiber Communication Conference (OFC), San Diego, CA, USA, 3–7 March 2019; p. Th2A.16. [CrossRef]
63. He, T.; Liu, Y.; Zhang, S.; Yan, Z.; Liu, D.; Sun, Q. High Accuracy Intrusion Pattern Recognition using a Dual-Stage-Recognition Network for Fiber Optic Distributed Sensing System. In Proceedings of the Conference on Lasers and Electro-Optics, Munich, Germany, 21–25 June 2021; p. JW1A.119. [CrossRef]
64. Liu, Y.; Wang, F.; Zhang, X.; Zhang, Y.; Xu, W.; Zhang, L. High performance interrogation by a composite-double-probe-pulse for ultra-weak FBG array. In Proceedings of the 17th International Conference on Optical Communications and Networks (ICOCN2018), International Society for Optics and Photonics. Bellingham, WA, USA, 14 February 2019. [CrossRef]
65. Liu, Y.; Li, H.; Liu, T.; Fan, C.; Yan, Z.; Liu, D.; Sun, Q. Polarization dependent noise suppression for fiber distributed acoustic sensor with birefringence estimation. In Proceedings of the Conference on Lasers and Electro-Optics: Applications and Technology, Washington, DC, USA, 10–15 May 2020; p. JW2E.18. [CrossRef]

66. Liu, T.; Li, H.; He, T.; Fan, C.; Yan, Z.; Liu, D.; Sun, Q. Fading Noise Free Distributed Acoustic Sensor Assisted with Double Wavelength lasers. In Proceedings of the Conference on Lasers and Electro-Optics: Applications and Technology, Anaheim, CA, USA, 23–25 October 2020; p. JW2E.10. [CrossRef]
67. Liu, Z.; Chen, D.W.; Xia, X.X.; Wang, G.Y.; Wang, X.S. A countering technique for LFM PC radar against shift-frequency jamming. *Mod. Radar* **2006**, *28*, 84–86. [CrossRef]
68. Zhou, Y.; Wang, C.; Wei, T.; Shangguan, M.; Xia, H. Simulation Research of Coherent Lidar Based on Golay Coding Technology. *Chin. J. Lasers* **2018**, *45*, 0810004. [CrossRef]
69. Jiang, J.; Xiong, J.; Wang, Z.; Qiu, Z.; Liu, C.; Deng, Z.; Rao, Y.-J. Quasi-Distributed Fiber-Optic Acoustic Sensing with MIMO Technology. *IEEE Internet Things J.* **2021**, *8*, 15284–15291. [CrossRef]
70. Wu, M.; Fan, X.; He, Z. Phase Noise Compensation for Ultra-highly Sensitive Fiber-optic Quasi-distributed Acoustic Sensing System. In Proceedings of the Conference on Lasers and Electro-Optics: Science and Innovations, San Jose, CA, USA, 5–10 May 2019. [CrossRef]
71. Wu, M.; Fan, X.; Liu, Q.; He, Z. Quasi-distributed fiber-optic acoustic sensing system based on pulse compression technique and phase-noise compensation. *Opt. Lett.* **2019**, *44*, 5969–5972. [CrossRef] [PubMed]
72. Wang, Z.T.; Jiang, J.L.; Xiong, J.; Wang, Z.N. Fiber-optic Quasi-distributed Acoustic Sensing System at Doubled Repetition Rate. In Proceedings of the Asia Communications and Photonics Conference (ACP), Chengdu, China, 2–5 November 2019; OSA Technical Digest (Optica Publishing Group). 2019; p. M4A.183.
73. Zhang, Y.X.; Fu, S.Y.; Chen, Y.S.; Ding, Z.W.; Shan, Y.Y.; Wang, F.; Chen, M.M.; Zhang, X.P.; Meng, Z. A visibility enhanced broadband phase-sensitive OTDR based on the UWFBG array and frequency-division-multiplexing. *Opt. Fiber Technol.* **2019**, *53*, 101995. [CrossRef]
74. Li, H.; Fan, C.; Liu, T.; Liu, Y.; Yan, Z.; Shum, P.; Sun, Q. Time-slot multiplexing based bandwidth enhancement for fiber distributed acoustic sensing. *Sci. China Inf. Sci.* **2021**, *65*, 119303. [CrossRef]
75. Li, Y.P.; Karrenbach, M.; Ajo, J. *Distributed Acoustic Sensing in Geophysics: Methods and Applications*; American Geophysical Union: Washington, DC, USA, 2022.
76. Li, C.; Mei, Z.; Cheng, C.; Tang, J.; Jiang, Y.; Yang, M. Draw Tower Grating-based Distributed Acoustic Sensing System and its Applications. In Proceedings of the Asia Communications and Photonics Conference, Chengdu, China, 2–5 November 2019; p. T2A.5. [CrossRef]
77. Li, T.; Fan, C.; Li, H.; He, T.; Qiao, W.; Shi, Z.; Yan, Z.; Liu, C.; Liu, D.; Sun, Q. Nonintrusive Distributed Flow Rate Sensing System Based on Flow-Induced Vibrations Detection. *IEEE Trans. Instrum. Meas.* **2021**, *70*, 7001808. [CrossRef]
78. Jiang, J.; Liu, F.; Wang, H.; Li, S.; Gan, W.; Jiang, R. Lateral positioning of vibration source for underground pipeline monitoring based on ultra-weak fiber Bragg grating sensing array. *Measurement* **2020**, *172*, 108892. [CrossRef]
79. Peng, Z.; Jian, J.; Wen, H.; Gribok, A.; Wang, M.; Liu, H.; Huang, S.; Mao, Z.-H.; Chen, K. Distributed Fiber Sensor and Machine Learning Data Analytics for Pipeline Protection against Extrinsic Intrusions and Intrinsic Corrosions. *Opt. Express* **2020**, *28*, 27277–27292. [CrossRef]
80. Fan, C.; Ai, F.; Liu, Y.; Xu, Z.; Wu, G.; Zhang, W.; Liu, C.; Yan, Z.; Liu, D.; Sun, Q. Rail Crack Detection by Analyzing the Acoustic Transmission Process Based on Fiber Distributed Acoustic Sensor. In Proceedings of the Optical Fiber Communication Conference, San Diego, CA, USA, 3–7 March 2019; p. Th2A.17. [CrossRef]
81. Hu, D.; Tian, B.; Li, H.; Fan, C.; Liu, T.; He, T.; Liu, Y.; Yan, Z.; Sun, Q. Intelligent Structure Monitoring for Tunnel Steel Loop Based on Distributed Acoustic Sensing. In Proceedings of the Conference on Lasers and Electro-Optics, Munich, Germany, 21–25 June 2021; p. ATh1S.4. [CrossRef]
82. Min, R.; Liu, Z.; Pereira, L.; Yang, C.; Sui, Q.; Marques, C. Optical fiber sensing for marine environment and marine structural health monitoring: A review. *Opt. Laser Technol.* **2021**, *140*, 107082. [CrossRef]
83. Lindsey, N.J.; Martin, E.R.; Dreger, D.S.; Freifeld, B.; Cole, S.; James, S.R.; Biondi, B.L.; Ajo-Franklin, J.B. Fiber-Optic Network Observations of Earthquake Wavefields. *Geophys. Res. Lett.* **2017**, *44*, 11792–11799. [CrossRef]
84. Jousset, P.; Reinsch, T.; Ryberg, T.; Blanck, H.; Clarke, A.; Aghayev, R.; Hersir, G.P.; Henninges, J.; Weber, M.; Krawczyk, C.M. Dynamic strain determination using fibre-optic cables allows imaging of seismological and structural features. *Nat. Commun.* **2018**, *9*, 2509. [CrossRef]
85. Sladen, A.; Rivet, D.; Ampuero, J.P.; De Barros, L.; Hello, Y.; Calbris, G.; Lamare, P. Distributed sensing of earthquakes and ocean-solid Earth interactions on seafloor telecom cables. *Nat. Commun.* **2019**, *10*, 5777. [CrossRef]
86. Lindsey, N.J.; Dawe, T.C.; Ajo-Franklin, J.B. Illuminating seafloor faults and ocean dynamics with dark fiber distributed acoustic sensing. *Science* **2019**, *366*, 1103–1107. [CrossRef] [PubMed]
87. Zhou, C.; Pang, Y.; Qian, L.; Chen, X.; Xu, Q.; Zhao, C.; Zhang, H.; Tu, Z.; Huang, J.; Gu, H.; et al. Demodulation of a Hydroacoustic Sensor Array of Fiber Interferometers Based on Ultra-Weak Fiber Bragg Grating Reflectors Using a Self-Referencing Signal. *J. Light. Technol.* **2018**, *37*, 2568–2576. [CrossRef]
88. Chen, J.F.; Li, H.; Liu, T.; Fan, C.Z.; Yan, Z.J.; Sun, Q.Z. Fully distributed hydroacoustic sensing based on lightweight optical cable assisted with scattering enhanced fiber. In Proceedings of the Optical Fiber Communication Conference (OFC), Washington, DC, USA, 6–11 June 2021; p. W7C.3. [CrossRef]